Radar Imaging of Moving Targets in Foliage Using Multifrequency Multiaperture Polarimetric SAR

Genyuan Wang, Xiang-Gen Xia, *Senior Member, IEEE,* and Victor C. Chen

***Abstract*—Because of the low signal-to-clutter ratio, it is a difficult problem to detect and image moving targets in foliage. In this paper, a multifrequency multiaperture polarimetric synthetic aperture radar (MFMA POLSAR) system is proposed for imaging of moving targets in foliage. The MFMA POLSAR extends the multifrequency antenna array SAR (MF-SAR) system to multiple polarizations. Full polarization is used in MFMA POLSAR to achieve an optimal polarization adaptive to the environment such that the images obtained by different apertures are of the best coherence that is used to obtain the highest accuracy of the phase estimation. It is also shown that the MFMA POLSAR cannot only accurately locate both the slow and the fast moving targets but also reveal moving targets in foliage.**

***Index Terms*—Foliage, moving targets, multifrequency, radar imaging, polarimetric, synthetic aperture radar (SAR).**

I. Introduction

SYNTHETIC aperture radar (SAR) imaging of moving targets in foliage has attracted much attention for both civilian and military applications, e.g., see [29], [32], and [33]. For SAR imaging of moving targets in foliage, there are two difficult problems. The *first problem* is SAR imaging of moving targets. It is known that moving targets are usually smeared and mislocated in a conventional SAR image [10]–[19]. For this problem, antenna array SAR has been proposed in, for example, [1]–[9], for slow moving-target imaging. Most recently, in [30], we studied the linear antenna array SAR and generalized it to a multiple-frequency system, called multifrequency linear antenna array SAR (MF-SAR). It is shown in [30] that the MF-SAR is able to accurately locate both slow and fast moving targets. The *second problem* is foliage. It is known that foliage reduces the signal (moving target) to clutter (stationary target) ratio (SCR). The reflectivity of foliage and targets depends on the environment as well as the radar polarization [29], [32]–[35]. Therefore, the accuracy of phase detection, which is needed for the detection of the motion parameters of the targets, also depends on the environment and the radar polarization. In this paper, we generalize the single-polarization MF-SAR system to a full-polarization system, where multiple polarization diversity is used to improve the SCR. Using the same idea proposed by Cloude and Papathanassiou [28], with the full-polarization data, an optimal polarization adaptive to the environment can be achieved such that the images obtained from different receivers reach the highest coherence. By combining the multiple polarizations and the multifrequency multiaperture, the multifrequency multiaperture polarimetric SAR (MFMA POLSAR) is able to accurately locate and image both the slow and the fast moving targets in foliage.

This paper is organized as follows. In Section II, MF-SAR imaging of moving targets is reviewed. In Section III, the MFMA POLSAR system is described. In Section IV, some simulation results are shown to illustrate the theory.

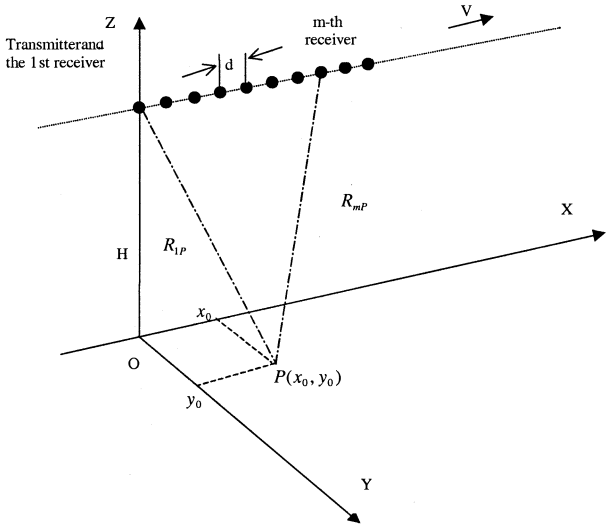

Fig. 1. Geometry of linear antenna array SAR.

II. MF-SAR Imaging of Moving Targets

In this section, we review the MF-SAR system proposed in [30] for moving-target imaging. Assume that the radar platform flies along a straight line with an altitude H and velocity v. The antennas are located along the direction of the flight track, where $M-1$ antennas are receiving, and one antenna is both transmitting and receiving; the distance between all the adjacent antennas is assumed d, as shown in Fig. 1.

A. Received Signals by Different Receivers

We define that the Y axis is along the projection of the radar line of sight on the horizontal plane and the X axis is the azimuth (or cross range) direction, which coincides with the flight

Manuscript received June 20, 2002; revised March 19, 2003. This work was supported in part by the 1998 Office of Naval Research (ONR) Young Investigator Program (YIP) Award under Grant N00014-98-1-0644 and ONR Grant N00014-0-110059 and the National Natural Science Foundation of China under Grant 60128102.

G. Wang and X.-G. Xia are with the Department of Electrical and Computer Engineering, University of Delaware, Newark, DE 19716 (e-mail: gwang@ee.udel.edu; xxia@ee.udel.edu).

V. C. Chen is with the Naval Research Laboratory, Washington, DC 20375 (e-mail: vchen@radar.nrl.navy.mil).

Digital Object Identifier 10.1109/TGRS.2003.813501

direction of the radar platform as shown in Fig. 1. The radar transmitter is assumed located at $x = 0$ in the X direction at time $t = 0$. The instantaneous coordinate (x, y) of the mth receiver at time t is

$$(x, y) = (vt + (m-1)d, 0). \tag{2.1}$$

Suppose that there is a point target P located at point (x_0, y_0) at time $t = 0$, and the target moves with a constant velocity (v_x, v_y). Suppose that the radar transmits a linear frequency modulated (LFM) signal with carrier frequency f_c and duration T

$$s(\tau) = \mathrm{Re}\left\{\exp\left[j2\pi\left(f_c\tau + \frac{\gamma}{2}\tau^2\right)\right]\right\}, \quad |\tau| < T/2 \tag{2.2}$$

where Re stands for the real part. The received signal at the mth receiver from the point scatterer P is

$$\begin{aligned} &s_{rm}(t, \tau) \\ &\quad = A_P s(\tau - t_{md}) \\ &\quad = \mathrm{Re}\left\{A_P \exp\left[j2\pi\left(f_c(\tau - t_{md}) + \frac{\gamma}{2}(\tau - t_{md})^2\right)\right]\right\} \end{aligned} \tag{2.3}$$

where τ is the fast time for the range dimension; t is the slow time for the cross-range dimension; c is the wave propagation velocity; A_P is the reflectivity of point P

$$t_{md} = \frac{R_{mP}(t)}{c} + \frac{R_{1P}(t)}{c} \tag{2.4}$$

and $R_{mP}(t)$ is the distance from the mth receiver of the radar to the point scatterer P at time t. See also (2.5) and (2.6), shown at the bottom of the page.

After mixing the received signal with transmitted signal and range compression [23]–[27] the signal $s_{rm}(t, \tau)$ becomes $s_m(t, \sigma)$ [30]

$$\begin{aligned} s_m(t, \sigma) = A_P \exp\left[-j\frac{2\pi(R_{mP}(t) + R_{1P}(t))}{\lambda}\right] \\ \cdot \mathrm{sinc}[\pi\gamma T_{cp}(\sigma - \tilde{t}_{md})]. \end{aligned} \tag{2.7}$$

Thus, the phase of the signal received at the mth antenna becomes

$$\begin{aligned} \phi_m(t) &= -\frac{2\pi(R_{mP}(t) + R_{1P}(t))}{\lambda} \\ &= -\frac{4\pi R_0}{\lambda} - \frac{2\pi}{R_0\lambda}[v^2t^2 + 0.5d^2(m-1)^2 + vt(m-1)d \\ &\qquad + v_x t(m-1)d + x_0(m-1)d \\ &\qquad + 2(x_0(v_x + v) + y_0 v_y)t \\ &\qquad + (v_x^2 + v_y^2 + 2vv_x)t^2]. \end{aligned} \tag{2.8}$$

B. Moving-Target VSAR Imaging

There are M receivers in the radar system. By normalizing the magnitude, from the mth antenna one can obtain a complex image as follows to a target located at (x_0, y_0) with velocity (v_x, v_y) in a range cell [30]

$$\begin{aligned} S_{m,(x_0,y_0)}(n) = \exp\left[-j\frac{4\pi R_0}{\lambda} - j\frac{2\pi}{R_0\lambda}(m-1)x_0 d\right] \\ \cdot\delta(n - n_{x_0} - \Delta_{\mathrm{shift}}) \end{aligned} \tag{2.9}$$

where n_{x_0} is the true imaging location in the cross range of the target with velocity zero, the shift Δ_{shift} is the shift/migration in the SAR image of the target from the true position n_{x_0} after the quantization by the SAR image resolution Δ_x because of the motion of the target, i.e.,

$$\Delta_{\mathrm{shift}} = \frac{\Delta}{\Delta_x} \tag{2.10}$$

and

$$\Delta = \frac{x_0 v_x + y_0 v_y}{v} \tag{2.11}$$

is shifted from the true position x_0. The *resolution* Δ_x of SAR image in the cross range depends only on the length of the synthetic aperture and the wavelength of the transmitted signal, which is therefore known. The target coordinate in the cross range can be determined by its image position in the corresponding direction. Thus

$$x_0 = \Delta_x n_{x_0} \tag{2.12}$$

where n_{x_0} is the image position of the target located at (x_0, y_0) with velocity $(v_x, v_y) = (0, 0)$. By multiplying the phase compensation function defined by

$$\begin{aligned} &\omega_\lambda(n_{x_0} + \Delta_{\mathrm{shift}}, m) \\ &\qquad = \exp\left[j\frac{2\pi}{R_0\lambda}(n_{x_0} + \Delta_{\mathrm{shift}})\Delta_x(m-1)d\right] \end{aligned} \tag{2.13}$$

to (2.9) and using $x_0 = \Delta_x n_{x_0}$, (2.9) becomes

$$\begin{aligned} S(m) &= S_{m,(x_0,y_0)}(n) \\ &= \exp\left[-j\left(\frac{4\pi R_0}{\lambda} - \frac{2\pi\Delta_x\Delta_{\mathrm{shift}}(m-1)d}{R_0\lambda}\right)\right] \\ &\quad \cdot \delta(n - n_{x_0} - \Delta_{\mathrm{shift}}) \end{aligned} \tag{2.14}$$

where m corresponds to the mth antenna receiver. To stationary target $(v_x, v_y) = (0, 0)$, $\Delta_{\mathrm{shift}} = 0$. In this case

$$S(m) = \exp\left(-j\frac{4\pi R_0}{\lambda}\right)\delta(n - n_{x_0}) \tag{2.15}$$

and the phases of the images are independent of an antenna m. However, for the moving targets, the phases of images de-

---

$$\begin{aligned} R_{mP}(t) &= [(x_0 + vt + v_x t + (m-1)d)^2 + (y_0 + v_y t)^2 + H^2]^{1/2} \\ &\approx R_0 + \frac{(v + v_x)^2t^2 + v_y^2t^2 + d^2(m-1)^2 + 2x_0(v + v_x)t + 2y_0v_yt + 2x_0(m-1)d + 2(v + v_x)(m-1)dt}{2R_0} \end{aligned} \tag{2.5}$$

where

$$R_0 = \sqrt{x_0^2 + y_0^2 + H^2} \tag{2.6}$$

pend on the antenna m as shown in (2.14). From (2.14), one can clearly see that the shift Δ_{shift} can be solved by taking the Fourier transform of $S(m)$, $1 \le m \le M$, with respect to variable m, under the condition that the shift Δ_{shift} is ***small enough*** such that there is no ambiguity due to the 2π modulo operation (folding) in the Fourier transform. The targets with different velocities may be in different image planes, which are called ***V-images***. This is basically the VSAR proposed in [1] and [2]. After Δ_{shift} being solved, the position n_{x_0} of the moving target can be, therefore, solved by subtracting Δ_{shift} from the detected position $n_{x_0} + \Delta_{\text{shift}}$. It can be seen from (2.14) that, for a stationary target, $\Delta_{\text{shift}} = 0$, i.e., the stationary target is in the 0th velocity image plane in the V-images. As we can see that, the above VSAR requires small value of Δ_{shift}, i.e., small-taret velocity, for the target location accuracy in the image.

C. Moving-Target MF-SAR Imaging

We now describe the principle of the MF-SAR system proposed in [30]. Assume the radar transmits signals with L different carrier wavelengths λ_i for $i = 1, 2, \ldots, L$. Consider the single moving target located at (x_0, y_0) with velocity (v_x, v_y). In this case, (2.14) becomes

$$S_i(m) = \exp\left[-j\left(\frac{4\pi R_0}{\lambda_i} - \frac{2\pi \Delta_{x,i}\Delta_{\text{shift},i}(m-1)d}{R_0\lambda_i}\right)\right] \tag{2.16}$$

and the detected positions are $n_{x_0} + \Delta_{\text{shift},i}$, $i = 1, 2, \ldots, L$. Then (2.10) becomes

$$\Delta_{\text{shift},i} = \frac{\Delta}{\Delta_{x,i}} \tag{2.17}$$

where Δ is defined in (2.11) and independent of an antenna and also independent of a signal wavelength, $\Delta_{x,i}$ and $\Delta_{\text{shift},i}$ are the cross-range resolution and the image shift/migration of the moving target with the wavelength λ_i, respectively. For $i = 1, 2, \ldots, L$, we define

$$f_i = \frac{\Delta_{x,i}\Delta_{\text{shift},i}d}{R_0\lambda_i}. \tag{2.18}$$

Then, for $i = 1, 2, \ldots, L$, from (2.16) we have

$$S_i(m) = \exp\left(-j\frac{4\pi R_0}{\lambda_i}\right)\exp\left[j\frac{2\pi M f_i(m-1)}{M}\right], \quad m = 1, 2, \ldots, M. \tag{2.19}$$

The DFT of $S_i(m)$ in terms of m gives the residue $\tilde{f}_i = f_i \bmod 1$ for $i = 1, 2, \ldots, L$. If $f_i < 1$, then $\tilde{f}_i = f_i$. In this case, there is no ambiguity for the estimated frequency f_i. Otherwise, there is an ambiguity on each estimated frequency from each S_i in (2.19) due to the modulo operation, i.e., the folding. We next want to see how the ambiguity can be resolved by using these multiple folded frequencies $\tilde{f}_i$, $i = 1, 2, \ldots, L$.

For each i, the estimate of the shift $\Delta_{\text{shift},i}$ of the target is the following residue

$$\tilde{\Delta}_{\text{shift},i} = \frac{\tilde{f}_i R_0\lambda_i}{\Delta_{x,i}d} = \Delta_{\text{shift},i} \bmod K_i \tag{2.20}$$

where

$$K_i = \frac{R_0\lambda_i}{\Delta_{x,i}d}. \tag{2.21}$$

When all the SAR image resolutions $\Delta_{x,i}$ are the same for all different wavelengths λ_i, from (2.17) we know that all the shifts $\Delta_{\text{shift},i}$ are the same, i.e., $\Delta_{\text{shift},i} = \Delta_{\text{shift}}$ for $i = 1, 2, \ldots, L$. In this case, to determine this shift is equivalent to determine its value from its L residues $\tilde{\Delta}_{\text{shift},i} = \Delta_{\text{shift}} \bmod K_i$ as in (2.20) for $i = 1, 2, \ldots, L$, which can then be solved by using the Chinese remainder theorem (CRT). In [30] we have discussed how to generate the images with the same resolution in the cross range from different wavelength λ_i, i.e., $\Delta_{x,i} = \Delta_x$, $i = 1, \ldots, L$, such that, $\Delta_{\text{shift},i} = \Delta_{\text{shift}}$, which is, therefore, always assumed in what follows.

By using the CRT, it is known that the maximal range of the detectable shift Δ_{shift} is

$$\begin{aligned}\max \Delta_{\text{shift}} &= \text{lcm}(K_1, K_2, \ldots, K_L) \\ &= \text{lcm}\left(\frac{R_0\lambda_1}{\Delta_x d}, \frac{R_0\lambda_2}{\Delta_x d}, \ldots, \frac{R_0\lambda_L}{\Delta_x d}\right)\end{aligned} \tag{2.22}$$

where lcm stands for the least common multiple. Clearly, if all the numbers $K_1, K_2, \ldots, K_L$ are co-prime each other, then the maximal range of the detectable shift Δ_{shift} is their product.

1) Three remarks: We want to mention here several things. The first remark is that, in the above CRT, the modulus $K_1, K_2, \ldots, K_L$ have to be integers. In [30], we have developed a robust CRT when they are not integers. The second remark is that in the above MF-SAR imaging, we assumed that there is only one moving point scatterer in a range and cross-range cell, which is true in most cases. When there are multiple moving point scatterer in a single range and cross-range cell, the above CRT does not apply. For this case, in [20]–[22] we have generalized the CRT for a single integer determination to a generalized CRT for a multiple integer determination from a sequence of residue sets. The third remark is the clutter rejection. As we have seen in Section II-B, all stationary clutter are in the zeroth V-image. To reject the clutter, we only need to delete the zeroth V-image, which may, however, delete some moving targets in the VSAR when their residues fall in the zeroth V-image. In [30], we have proved that, in the MF-SAR, the deletion of the zeroth V-images in the L many V-image sequences does not eliminate any moving target in all the L V-image sequences, i.e., the MF-SAR imaging of moving targets is also robust to the clutter rejection.

III. MFMA POLSAR Imaging of Moving Targets in Foliage

As we have seen in the previous section, moving-target imaging is obtained by the phase estimation and therefore the accuracy of the phase estimation determines the image quality. It is clear that the phase estimation accuracy is determined by the SNR that is usually low in foliage applications due to the clutter reflection. The foliage reflectivity depends on the system parameters, such as polarizations, as well as physical and geometrical parameters of the scatter. This is similar to interferometry SAR, where the phase is used for the height estimation. The polarimetric interferometry SAR system was proposed by Cloude and Papathanassiou [28] to improve the SNR by using full polarization instead of a single polarization. In what follows, we use the same idea as in [28] and propose

multifrequency and multiaperture polarimetric SAR (MFMA POLSAR), where the full polarization is used to improve the SCR and therefore the SNR in the phase estimation. The difference between the moving-target SAR imaging and the interferometric SAR imaging is the clutter treatment, where the clutter in interfermetric SAR is signal while it is noise in moving-target SAR imaging as we shall see the details later.

A. Relationship Between Phase Estimation and Coherence of Images

In MFMA POLSAR, at each slow time sample point, both H and V polarization waveforms are sent by the transmitter, and the signals are also received with both H and V polarizations at each receiver. With the wavelength λ_i, at the mth receiver a full-polarization complex SAR image

$$[S]_{m,i} = \begin{bmatrix} S_{\mathrm{HH}_{m,i}} & S_{\mathrm{HV}_{m,i}} \\ S_{\mathrm{VH}_{m,i}} & S_{\mathrm{VV}_{m,i}} \end{bmatrix}$$

can be obtained.

Before we study the optimal polarization, let us first see the relationship between phase estimation and the coherence of images obtained in an antenna array. Consider two radar signals s_1 and s_2 from two receive antennas observing the same target at the same time (for example, two images with the same polarization and wavelength but from two receivers). If we model signals consisting of a correlated part r common to the signals at both antennas and uncorrelated parts n_1 and n_2 (noises are uncorrelated parts because of the position differences of antennas and foliage):

$$s_1 = r + n_1, \tag{3.1a}$$

$$s_2 = r\exp(j\varphi_0) + n_2 \tag{3.1b}$$

then phase φ_0, which is what we need, can be estimated as

$$\tilde{\varphi}_0 = \arctan\left(\frac{\mathrm{Im}\{s_1^* s_2\}}{\mathrm{Re}\{s_1^* s_2\}}\right) + 2N\pi, \qquad N \text{ is an integer.} \tag{3.2}$$

Because

$$\begin{aligned} s_1^* s_2 &= r^* r\exp(j\varphi_0) + r^* n_2 + n_1^* r\exp(j\varphi_0) + n_1^* n_2 \\ &= r^* r\left\{\exp(j\varphi_0) + \frac{n_2}{r} + \frac{n_1^*\exp(j\varphi_0)}{r^*} + \frac{n_1^* n_2}{r^* r}\right\} \\ \exp(j\varphi_0) &= \frac{s_1^* s_2}{|r|^2} - \left\{\frac{n_2}{r|r|^2} + \frac{n_1^*\exp(j\varphi_0)}{r^*|r|^2} + \frac{n_1^* n_2}{|r|^4}\right\} \\ &= \frac{s_1^* s_2}{|r|^2} + o(\mathrm{SNR}^{-1}) \end{aligned} \tag{3.3}$$

where n_1 and n_2 are independent of the signals and have the same variance $E(n*n)$, and $o(x)$ goes to 0 as x goes to 0. The larger the SNR (SNR $= E(r*r)/E(n*n)$) is, the more accurate the estimation $\tilde{\varphi}_0$ of phase φ_0 is. In general, the SNR cannot be estimated directly. However, it has a close relationship with the correlation coefficient ρ between two received signals s_1 and s_2

$$\rho = \frac{\langle s_1^* s_2\rangle}{\sqrt{\langle s_1^* s_1\rangle\langle s_2^* s_2\rangle}} = \frac{E(r*r)}{E(r*r)+E(n*n)} = \frac{1}{1+\mathrm{SNR}^{-1}} \tag{3.4}$$

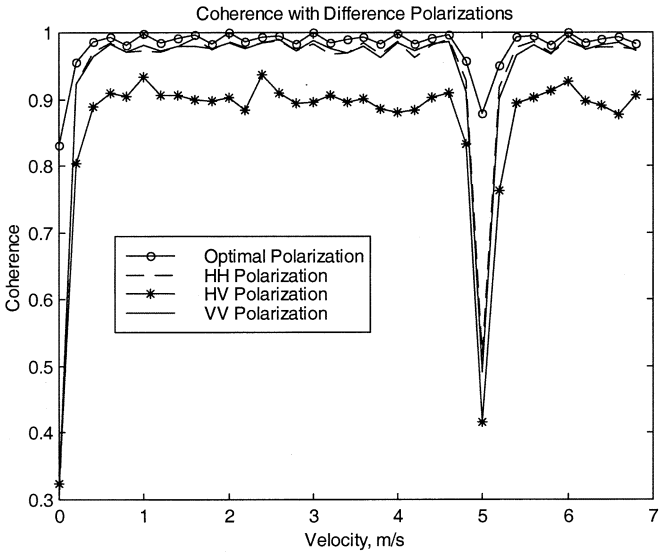

Fig. 2. Image coherence with different polarizations.

where $\langle\bullet\rangle$ denotes the ensemble average. Therefore, *the higher the correlation ρ between two received signals s_1 and s_2 is, the more accurate the estimated phase φ_0 is*. We next discuss how to obtain a higher correlation of the images obtained from different antennas.

B. Optimal Polarization for Moving Targets

As we mentioned before, SCR not only depends on target characteristics but also on a polarization of a transmitted signal. Fig. 2 shows the coherence results of images with different polarizations in an environment, where one can clearly see that different polarizations produce different coherences of images. In what follows, we want to find the optimal polarization in a given environment such that the images of moving targets have the highest coherence.

Since any polarization can be obtained by a linear combination of a set of orthogonal polarizations, to obtain an optimal polarization is to find an optimal linear combination from a set of orthogonal polarizations, e.g., see [28] and [29]. For convenience, we use the same notations as in [28]. For a full-polarization radar system, a 2×2 complex scatterering matrix

$$[S] = \begin{bmatrix} S_{\mathrm{HH}} & S_{\mathrm{HV}} \\ S_{\mathrm{VH}} & S_{\mathrm{VV}} \end{bmatrix} \tag{3.5}$$

for each cell in an image can be obtained. In the case of backscatterering in a reciprocal medium, the reciprocity theorem implies the scattering matrix to be *complex symmetric*, i.e., $S_{\mathrm{HV}} = S_{\mathrm{VH}}$. Therefore, from the 2×2 complex scatterering matrix $[S]$ we obtain a three-dimensional (3-D) scatterering vector

$$\mathbf{k} = [S_{\mathrm{HH}}, S_{\mathrm{HV}}, S_{\mathrm{VV}}]^T \tag{3.6}$$

where T stands for the transpose.

Consider a linear combination $\mu = \mathbf{w}^*\mathbf{k}$ as a "new polarization," where $\mathbf{w}$ is a normalized complex vector of norm 1. From two vectors $\mathbf{k}_1$ and $\mathbf{k}_2$ corresponding to two adjacent antennas, we have two linear combinations $\mu_1 = \mathbf{w}_1^*\mathbf{k}_1$ and $\mu_2 = \mathbf{w}_2^*\mathbf{k}_2$.

Then, μ_1 and μ_2 are used to estimate the desired signal phase difference of the two antennas as

$$\tilde{\varphi}_0 = \arctan\left(\frac{\mathrm{Im}\{\mu_1^*\mu_2\}}{\mathrm{Re}\{\mu_1^*\mu_2\}}\right) + 2N\pi, \qquad N \text{ is an integer.} \tag{3.7}$$

The accuracy of the estimation $\tilde{\varphi}_0$ of φ_0 depends on the choices of weights w_1 and w_2. The optimal weights $w_{1,0}$ and $w_{2,0}$ are the ones such that their corresponding polarizations $\mu_{1,0} = \mathbf{w}_{1,0}^*\mathbf{k}_1$ and $\mu_{2,0} = \mathbf{w}_{2,0}^*\mathbf{k}_2$ have the largest coherence

$$[\mathbf{w}_{1,0}, \mathbf{w}_{2,0}] = \underset{\mu_1,\mu_2}{\mathrm{argmax}} \frac{\mu_1^*\mu_2}{\sqrt{\mu_1^*\mu_1\mu_2^*\mu_2}}. \tag{3.8}$$

Cloude and Papathanassiou [28] presented an algorithm to solve the above optimal problem for interferometry SAR imaging. In the following, we develop a similar algorithm for moving-target imaging, where the clutter is no longer signal but noise and therefore needs to be rejected in the first place.

1) Clutter Rejection: The signal model

$$s_1 = r + n_1 \tag{3.9a}$$

$$s_2 = r\exp(j\varphi_0) + n_2 \tag{3.9b}$$

used in [31] means that received signals are target signals corrupted with additive noises. With the polarimetric SAR interferometry [28], target signals are the signals reflected from clutter, where an image pixel may contain several clutters with possibly different heights and the phase difference φ_0 represents an average height of these clutters. In general, it is hard to obtain the height information of each clutter from the phase difference φ_0, which is, however, not serious in interferometry SAR imaging because the height differences of the clutters imaged in an image pixel are usually not large due to the clutters are close to each other in one image pixel. This is different in moving-target imaging, where an image pixel with a moving target usually contains both moving target and clutter. In this case, the velocity of a moving target may be large and the averaged phase or velocity of a moving target and clutters may be much different from the moving-target velocity. Furthermore, the signal (a moving target) to clutter (stationary targets) ratio is low, and in order for the signal model in (3.9a) and (3.9b) to work, we first separate the signals of a moving target and stationary targets, i.e., clutter rejection. Note that, because the probability of two or more moving targets are imaged in a single range and cross-range cell is small, we only consider the case of a single moving target in an image cell or pixel.

From (2.19), after the phase compensation, the obtained images from the ith wavelength and the different receivers can be expressed as

$$\begin{aligned} S_i(m) &= r_s + r_{mv}\exp\left[j\frac{2\pi M f_i(m-1)}{M}\right] + n_m \\ &= r_{m,i}\exp(j\varphi_{m,i}) + n_m, \qquad m = 1, 2, \ldots, M \end{aligned} \tag{3.10}$$

where r_s is the complex image of stationary targets; r_{mv} is the complex image of a moving target; and n_m is the measurement noise of the mth receiver

$$r_{m,i} = \sqrt{|r_s|^2 + |r_{mv}|^2 - 2|r_s||r_{mv}|\cos\theta_m} \tag{3.11}$$

$$\theta_m = 2\pi f_i(m-1) \tag{3.12}$$

$$\varphi_{m,i} = \arctan\left\{\frac{r_{mv}\sin(2\pi f_i(m-1))}{|r_s| + |r_{mv}\cos(2\pi f_i(m-1))|}\right\}. \tag{3.13}$$

Note: The term r_s in (3.10) is, in fact, comprised of mixed surface and volume scattering terms depending on the wavelength and extinction by the vegetation. In the across track interferometry as in [28] the optimizer also adjusts the ratio of the surface to volume scattering so as to maximize the coherence. Since the volume scattering is vertically distributed, its coherence changes as a function of baseline. In this paper, MFMA SAR for moving-target detection can be thought of as an along track interferometry. In this case, the volume-decorrelation is not as serious as that in [28]. However, the difference of view angles of different antennas can also induce some decorrelations of r_s, which depends on the wavelength and polarization. Borrowing the idea from [28], we optimize the polarization to improve the correlation of r_s from different antennas in moving-target detection.

Since r_s may be generated from several stationary targets, it is usually greater than r_{mv}. This implies that, even when there is no noise n_m in (3.10), the detected phase $\varphi_{m,i}$ is much different to the desired phase θ_m. The optimal polarization algorithm in [28] is to find an optimal polarization such that the ratio of $r_{m,i}$ over n_m is the largest, which only aims for the estimation of $\varphi_{m,i}$ but not for θ_m. Therefore, we need to develop a different algorithm.

To estimate $2\pi f_i$, i.e., the second part in (3.10), the term

$$r_{mv}\exp\left[j\frac{2\pi M f_i(m-1)}{M}\right]$$

is the desired one and we need to suppress the first part r_s. Different from the third random part n_m in (3.10), for a fixed polarization the first part is constant to all the antennas and therefore can be removed by taking a highpass filter along the antenna direction m. The signal from a moving target remains if it is not imaged in the zeroth image plane in V-images for a fixed wavelength. It is proved in [30] that a moving target cannot be imaged in all the zeroth images in L V-image sequences in MF-SAR. Therefore, a moving target cannot removed from the highpass filtering in the antenna array direction for all wavelengths. We now first consider the case when clutter is removed and a target is remained. After the clutter rejection, the signal (moving target) to clutter (stationary targets plus noise) is improved. Then, for each polarization l = HH, HV, VV, (3.10) becomes

$$S_{i,l}(m) = r_{mv}\exp\left[j\frac{2\pi M f_i(m-1)}{M}\right] + w_m \tag{3.15}$$

where w_m is the sum of original noise n_m and the residue signal of the stationary clutter.

2) Moving-Target Detection and Velocity Estimation: After the clutter is removed, (3.15) is the same as the one in model (3.1). Then, the optimal polarization algorithm developed in [28] can be applied. The problem now is how to get statistical data of the signal to estimate the optimal polarization? In [28], multilook is used. Since multilook usually reduces the resolution of an image and a moving target is a point target, multilook approach might not be a good method to obtain multiple

statistical data. In this paper, we propose to use statistical data from the antenna diversity of a linear antenna array system. For each polarization l, (l = HH, HV, or VV) and wavelength λ_i, we have M complex images $S_{i,l}(m)$ from (2.19). Using the M images we can generate $M-1$ signals

$$s_{i,l}(m) = S_{i,l}(m)^* S_{i,l}(m+1), \qquad m = 1, 2, \ldots, M-1 \tag{3.16}$$

where $s_{i,l}(m)$ has the same model as in (3.1) with phase $\varphi_0 = 2\pi f_i$ as we have seen from the previous subsection, and $s_{i,l}(m)$. These $M-1$ antenna pairs are used to estimate optimal polarizations $\mathbf{w}_{1,i}$ and $\mathbf{w}_{2,i}$. To estimate $\mathbf{w}_{1,i}$ and $\mathbf{w}_{2,i}$, the coherence estimation requires an average of the independent samples between antenna pairs. For large M, for example 10, the antennas can be separated into two groups: odd numbers and even numbers. The images in each group are independent, which can be used as independent samples to estimate the coherence. For small M, we can also separate the images $s_{i,l}(m) = S_{i,l}(m)^* S_{i,l}(m+1)$, $m = 1, 2, \ldots, M-1$, to estimate the coherence. In this case, the samples between antenna pairs are not totally independent. However, we have done some simulations on M random variable $[x_1, x_2, \ldots, x_M]$ and find that the correlation level of $[x_1, x_2, \ldots, x_{M-1}]$ with $[x_2, x_3, \ldots, x_M]$ is similar to that of $[x_1, x_3, \ldots, x_{M-1}]$ with $[x_2, x_4, \ldots, x_M]$ in this application.

What we need to mention here is that the optimal polarizations $\mathbf{w}_{1,i}$ and $\mathbf{w}_{2,i}$ obtained by the algorithm in [28] may depend on the wavelength λ_i, and therefore the optimal polarizations $\mathbf{w}_{1,i}$ and $\mathbf{w}_{2,i}$ should be estimated separately in terms of different wavelengths λ_i. There are two methods to estimate the phase difference $2\pi f_i$. The first method is to obtain $M-1$ estimates from each adjacent antenna pair, and then to obtain a more accurate estimate by averaging these $M-1$ estimates. The other method is to obtain the signal sequence $\{x_i(m)\}_{m=1}^{M}$ with the optimal weights $\mathbf{w}_{1,i}$ and $\mathbf{w}_{2,i}$ obtained in (3.16)

$$x_i(m) = (\mathbf{w}_{1,i}^* \mathbf{k}_{1,i})^* (\mathbf{w}_{2,i}^* \mathbf{k}_{m,i}) \tag{3.17}$$

which is used to estimate the velocity information of the moving target by using the MF-SAR in [30], where $\mathbf{k}_{m,i}$ are the polarization vectors

$$\mathbf{k}_{m,i} = [S_{i,\mathrm{HH}}(m),\ S_{i,\mathrm{HV}}(m),\ S_{i,\mathrm{VV}}(m)]^T \tag{3.18}$$

where $S_{i,l}(m)$ is of the form (3.15). Signal $x_i(m)$ is a sinusoidal signal corrupted by noise, and the frequency of the sinusoidal signal is $2\pi f_i$, which can be estimated by taking the M-point discrete Fourier transform of $\{x_i(m)\}_{m=1}^{M}$ in terms of m similar to obtaining V-images in MF-SAR. The difference between the MF-SAR (2.19) and (3.17) is that a single polarization is used in (2.19) while an optimal combination ("polarization") is used in (3.17) where the full-polarization data are adopted.

The above phase detection is done for each wavelength. Although as we mentioned earlier that a moving target cannot be removed in all the L V-image sequences of all wavelengths, it may be removed in V-images from an individual wavelength. In this case, both clutter and target are removed in the highpass filtering of the clutter rejection and thus the estimated phase for the moving target is not correct because the phase is not coming from the moving target but from the noise. Therefore, before obtaining the optimal polarization and the phase estimate, a decision is made to determine whether a moving target is removed or not. The decision is made by comparing the signal energies of the signal before and after the highpass filtering. If the latter one is small enough compared to the former one, it is decided that a moving target has been removed, i.e., a moving target is imaged at the zeroth image plane in the V-images of a wavelength. In this case, the phase estimate is 0. After all the phases from all the V-images of all wavelengths are estimated, the true moving-target locations are then estimated using the robust CRT developed in [30].

Remark: There are three different polarizations. In the above decision making of whether a moving target is removed in the clutter rejection, we use a combination of the three polarizations. It should be noted that the weights used for the optimal polarization may not be the best one for the above decision making. The weights used in this paper to decide whether a moving target is removed in the clutter rejection are the ones that normalize the signal energies with different polarizations, i.e., normalize the polarimetric $\mathbf{k}_{m,i}$ by its total power

$$\tilde{w}_{m,i} = \frac{k_{m,i}}{\|k_{m,i}\|^2} \tag{3.19}$$

where the linear combination of the full polarizations for the moving-target detection is $\tilde{w}_{m,i} \bullet \mathbf{k}_{m,i}$, and m stands for the mth antenna and i stands for the ith wavelength.

IV. Simulation Results

In our simulations, the canopy penetration model in [28] is used.

A. Simulation Model

Consider a pair of receiver antennas: antenna 1 and antenna 2. The 3-D complex vectors $\mathbf{k}_1$ and $\mathbf{k}_2$ have the following model [28]:

$$\mathbf{k}_1 = \exp(2\boldsymbol{\kappa} \bullet \mathbf{r}_{T_1})\mathbf{k}_T + \int_V \exp(2\boldsymbol{\kappa} \bullet \mathbf{r}_1)\mathbf{k}(\mathbf{r}_1)\, d\mathbf{r}_1 \tag{4.1a}$$

$$k_2 = \exp(2\boldsymbol{\kappa} \bullet r_{T_2})k_T + \int_V \exp(2\boldsymbol{\kappa} \bullet r_2)k(r_1)\, dr_2 \tag{4.1b}$$

where $\boldsymbol{\kappa}$ is the complex wave-number of the propagation and represents both attenuation and phase shift in the medium, $\mathbf{r}_{T_i}$ and $\mathbf{r}_i$ represent the locations of target and clutter with respect to the ith receiver, respectively, V represents the set of clutters contained in an image pixel, and $\mathbf{k}_T$ and $\mathbf{k}_{r_i}$ represent the complex polarization vectors of target and clutter modeled in [28], respectively. The above model is for the interferometry SAR. There is a difference with the moving-target SAR as follows. After the phase compensation in (2.14), the phase shifts of each target and clutter depend on the product $r_x v_y$ of the target (clutter) location r_x in the radar sight direction and the velocity v_y of the target (clutter) in the light of radar sight direction, while in [28], the phase shift depends only on the clutter location. Therefore, the model used in our simulation is modified from the above model and is as follows:

$$\mathbf{k}_{i,m} = \phi_{i,m}(\mathbf{r}_{T_m})\mathbf{k}_T + \int_V \phi_{i,m}(\mathbf{r}_m)\mathbf{k}(\mathbf{r}_m)\, d\mathbf{r}_m \tag{4.2}$$

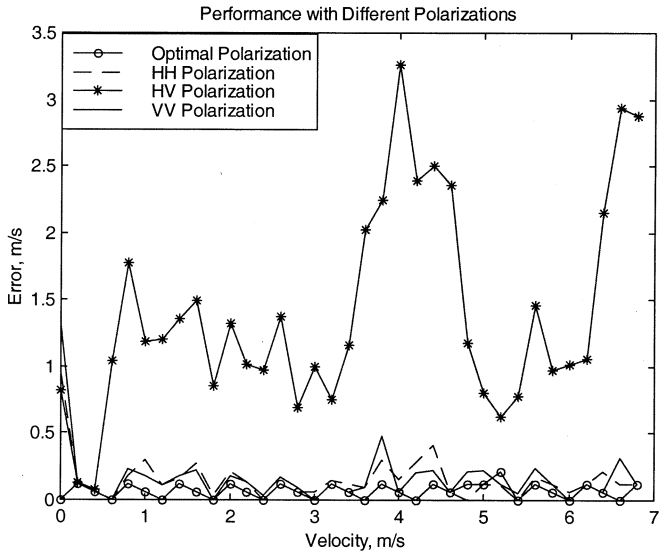

Fig. 3. Velocity estimate errors with different polarizations.

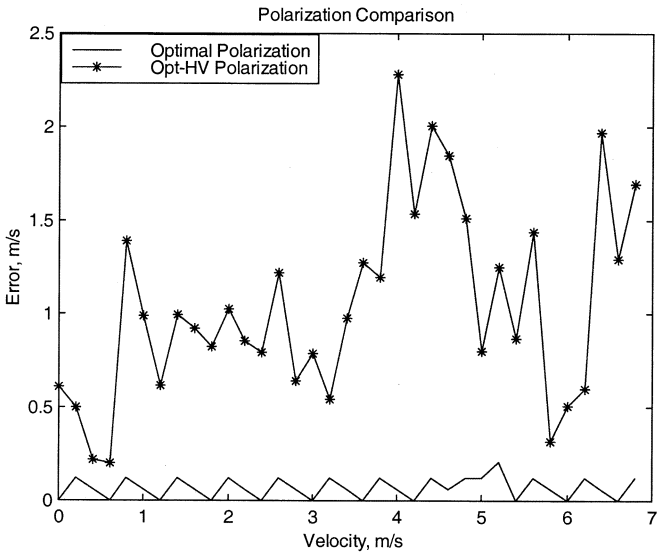

Fig. 4. Effect of polarization to the velocity estimation.

where

$$\phi_{i,m}(\mathbf{r}_{T_m}) = \exp\left[-j\left(\frac{4\pi R_{\mathbf{r}_{T_m}}}{\lambda_i} - \frac{2\pi\Delta_{x,i}\Delta_{\text{shift},i}(m-1)\,d}{R_{\mathbf{r}_{T_m}}\lambda_i}\right)\right] \quad (4.3)$$

$$\phi_{i,m}(\mathbf{r}_m) = \exp\left(-j\frac{4\pi R_{\mathbf{r}_m}}{\lambda_i}\right) \quad (4.4)$$

where i stands for the ith carrier frequency f_i; m stands for the mth receiver.

B. Simulation Parameters and Results

In our simulations, there are ten random clutter scatters in an image pixel (per cell). The polarimetric characteristics of the clutter obeys the model described in [28], and α and β in [28] for each scatter are randomly chosen. The clutter reflectivity obeys the uniform distribution on the interval $[0, 1]$ and the noise is

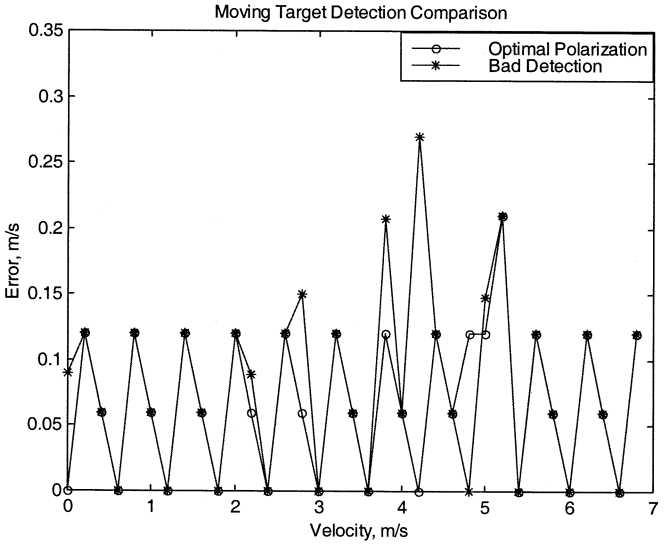

Fig. 5. Effect of moving-target detection on velocity estimation.

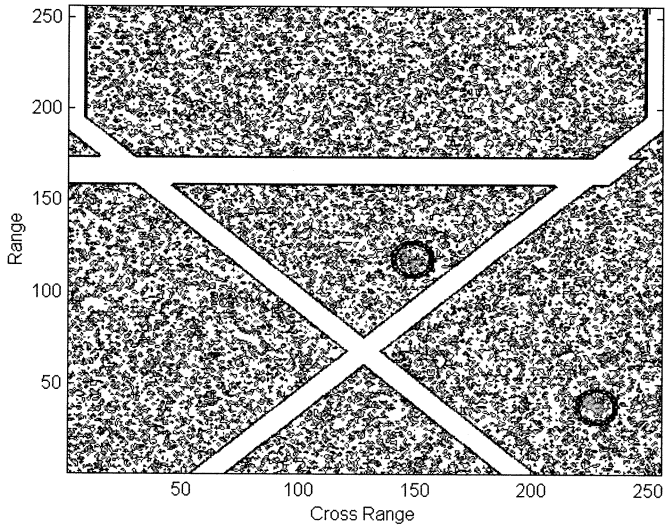

Fig. 6. Conventional SAR imaging result.

additive white Gaussian noise (AWGN) with mean 0 and variance 0.1. The moving-target reflectivity is three with the choice of $\alpha = \pi/4$, $\beta = \pi/3$ in the module [28]. The distance of the radar to the image area is about 10 000 m. Two wavelengths are used: $\lambda_1 = 0.07$ m and $\lambda_2 = 0.05$ m. There are $M = 10$ receivers in the system and the distance between the adjacent antennas is $d = 2$ m.

Fig. 2 shows the simulation on coherence results of images with different polarizations and velocities of moving targets after the clutter is removed. From this figure we can find that the coherences are different with different polarizations. The coherence with the optimal polarization is the highest one. This means that the reflectivity of the vegetation is more sensitive to the view angle change for some specific polarization. And this is the reason why by choosing optimal polarization the coherence of images from different antennas and therefore the capability of moving-target detection can be improved. The coherence at some velocities, such as the velocities around 0 and 5 m/s, are lower than others. This is because the target is

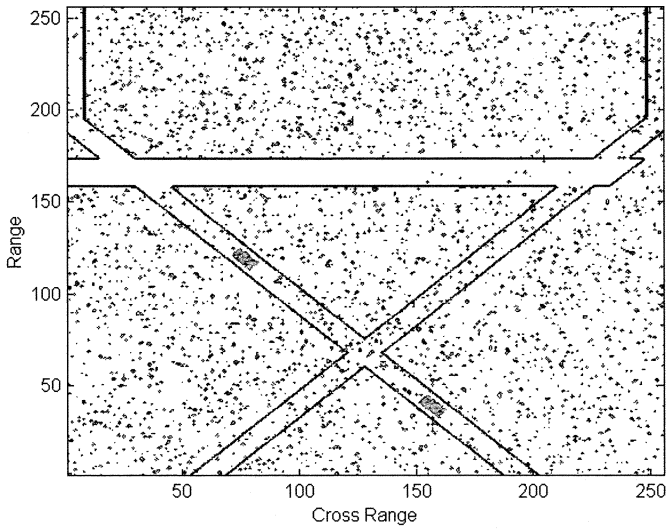

Fig. 7. MF-SAR imaging with HV polarization.

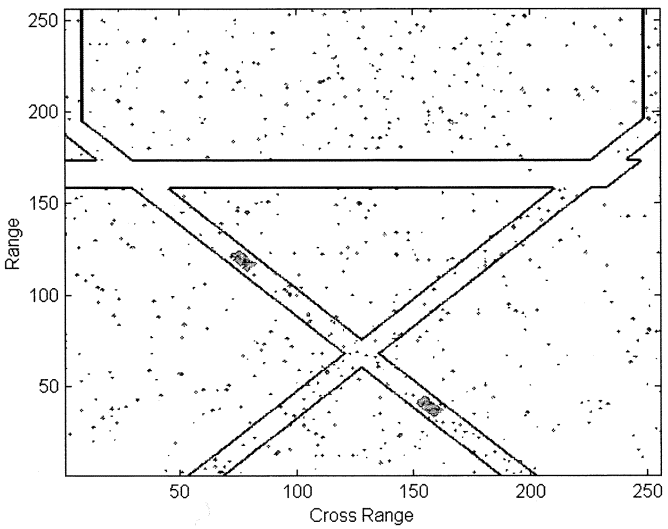

Fig. 9. MF-SAR imaging with VV polarization.

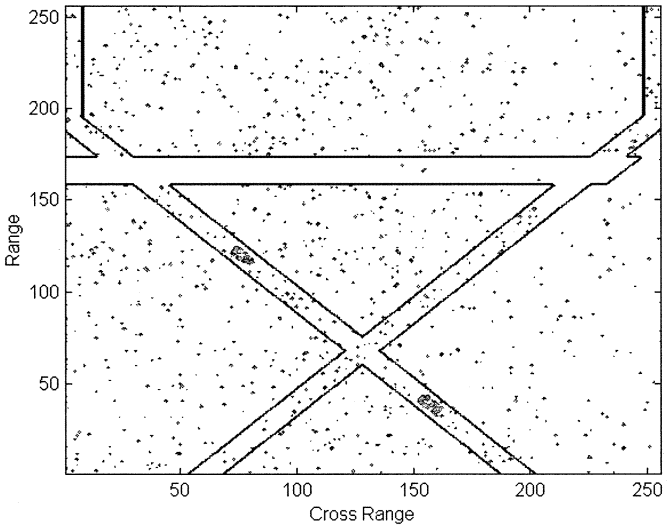

Fig. 8. MF-SAR imaging with HH polarization.

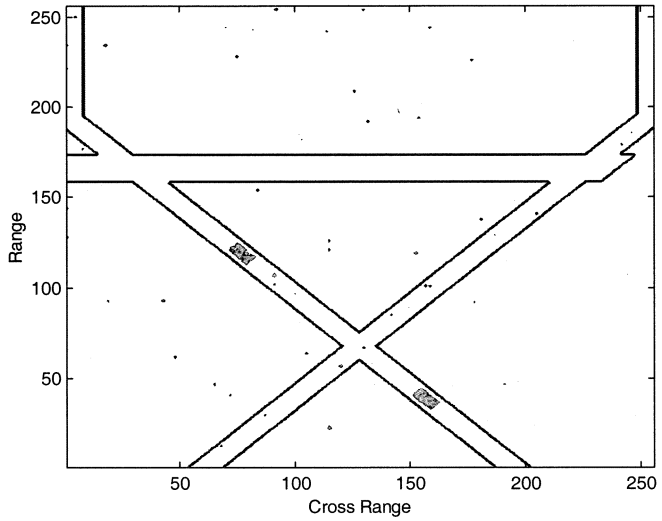

Fig. 10. MFMA POLSAR imaging.

imaged in both cases (for the velocity 5 m/s, it is folded to the zeroth image in V-images) close to the zeroth frequency image plane (the image plane of stationary targets) due to the phase ambiguity, and some energy of the moving target is removed. In this case, the SNR is reduced.

Figs. 3–5 show some comparisons of the velocity estimation of moving targets in foliage. The velocities of moving targets are between 0–7 m/s in the range direction. These simulation results are statistical results by performing 100 random trials of environment. Fig. 3 shows the velocity estimation errors by using the MF-SAR with a single polarization of HH, HV, and VV, and the MFMA POLSAR system with the optimal polarization. As studied in Section III-B.2, two procedures are used in the MFMA POLSAR system proposed in this paper: one is the detection whether a moving target is removed in the clutter rejection (for convenience, we name it later as *moving-target detection*) and the other is the phase estimation from the full polarizations. In these two procedures, the weights of linear combinations of the different polarizations may be different as mentioned in Remark at the end of the last section: for the moving-target detection we use the normalized weights (3.19) and for the phase estimation we use the optimal polarization (3.8). Fig. 4 shows the effect of the polarization on the velocity estimation errors, where the curve marked by solid line shows the velocity estimation errors using (3.19) in the moving-target detection and the optimal polarization (with the highest image coherence) (3.8), and the curve marked by $*$ shows the velocity estimation errors by using the same moving-target detection method but the HV polarization. From Fig. 4, one can see the difference the optimal polarization makes on the velocity estimation. Fig. 5 shows the effect of the moving-target detection on the velocity estimation, where the curve marked by $*$ shows the velocity estimation errors by using the optimal polarization weights (3.8) in both the moving-target detection and the phase estimation, and the curve marked by o shows the velocity estimation errors by using the normalized weights (3.19) in the moving-target detection and the optimal polarization (3.8) in the

phase estimation. From Fig. 5, one can see that the optimal polarization weights (3.8) for the moving-target detection (bad detection) may not be as good as the normalized weights (3.19).

We next simulate moving-target imaging in foliage. In the following simulations, two moving targets are located at around the 40th and 120th range cells with velocity 4.2 m/s in the range direction on the road. In order to show the imaging results better, each of the two moving targets consists of many point reflectors, and three roads are generated. Fig. 6 shows the conventional SAR imaging result, where the data of the VV polarization is used and the two moving targets are circled manually since both of them are imaged off the road. The layover has been ignored (some vegetation from the top of the canopy should be imaged on the road) in Fig. 6. The imaging results of the MF-SAR system proposed in [30] with HV polarization, HH polarization and VV polarization of the moving targets in foliage are shown in Fig. 7, Fig. 8 and Fig. 9, respectively, where one can see that the moving targets are correctly imaged on the road but there are other clutters also imaged on the roads. Fig. 10 shows the MFMA POLSAR imaging result of the same data used in Figs. 7–9, where one can see the image quality is clearly improved and much less clutters are imaged on the roads.

V. Conclusion

In this paper, we have proposed a multifrequency and multiaperture polarimetric SAR (MFMA POLSAR) imaging system of moving targets in foliage. In the MFMA POLSAR, the radar transmits full-polarization waveforms with multiple wavelengths, and the receivers receive the signal with full polarization, which is a generalization of the MF-SAR [30]. By using the polarimetric diversity, higher SCR can be obtained through an adaptive optimal polarization such that a higher accurate phase estimate of a moving target can be obtained comparing to a single-polarization system. Some simulation results based on the polarization model proposed in [28] have been presented to illustrate the theory.

References

[1] B. Friedlander and B. Porat, "VSAR: A high resolution radar system for detection of moving targets," *Proc. Inst. Elect. Eng.—Radar, Sonar Navigat.*, vol. 144, no. 4, pp. 205–218, 1997.

[2] ——, "VSAR: A high resolution radar system for ocean imaging," *IEEE Trans. Aerospace Electron. Syst.*, vol. 34, pp. 755–776, July 1998.

[3] J. Ender, "Detectability of slowly moving targets using a multi-channel SAR with an along-track antenna array," in *Proc. SEE/IEE Conf. (SAR 93)*, Paris, France, May 1993, pp. 19–22.

[4] ——, "Detection and estimation of moving target signals by multi-channel SAR," in *Proc. EUSAR'96 Conf.*, 1996, pp. 411–417.

[5] W. Rieck, "SAR imaging of moving targets: application of time-frequency distribution for single- and multi-channel data," in *Proc. EUSAR'96 Conf.*, 1996, pp. 431–434.

[6] P. Lombardo, "Estimation of target motion parameters from dual-channel SAR echoes via time-frequency analysis," in *Proc. National Radar Conf.*, 1997, pp. 13–18.

[7] G. Wang, X.-G. Xia, and V. C. Chen, "Dual-speed SAR imaging of moving targets," Dept. of Electrical and Comput. Eng., Univ. Delaware, Tech. Rep. UDEL 98-8-1, 1998. This also appears in *Proc. 1999 IEEE Radar Conf.*, pp. 227–232.

[8] S. Barbarossa and A. Farina, "Detection and imaging of moving targets with synthetic aperture radar. Part 2: Joint time-frequency analysis and Wigner–Ville distribution," *Proc. Inst. Elect. Eng.*, pt. F, vol. 139, pp. 89–97, Feb. 1992.

[9] ——, "Space-time-frequency processing of synthetic aperture radar signals," *IEEE Trans. Aerospace Electron. Syst.*, vol. 30, pp. 341–358, Apr. 1994.

[10] F. Berizzi and M. Diani, "Target angular motion effects on ISAR imaging," *Proc. Inst. Elect. Eng.—Radar, Sonar Navigat.*, vol. 144, no. 2, pp. 87–95, 1977.

[11] W. G. Carrara, R. S. Goodman, and R. M. Majewski, *Spotlight Synthetic Aperture Radar—Signal Processing Algorithms*. Norwood, MA: Artech House, 1995.

[12] A. Moreira, R. Scheiber, and J. Mittermayer, "Azimuth and range scaling for SAR and scan SAR processing," in *Proc. IGARSS*, 1996, pp. 1214–1216.

[13] V. C. Chen, "Time-frequency analysis of SAR image with ground moving targets," in *Proc. SPIE*, vol. 3391, Orlando, FL, Apr. 1998, pp. 295–302.

[14] W. Xu, E. C. Chang, L. K. Kwoh, H. Lim, and W. C. A. Heng, "Phase-unwrapping of SAR interferogram with muti-frequency or multi-baseline," in *Proc. IGARSS*, 1994, pp. 730–732.

[15] K. Schnitt and W. Wiesbeck, "An interfermetric SAR processor avoiding phase ambiguities," in *Proc. IGARSS*, 1997, pp. 1713–1715.

[16] H. Shnitkin, "Joint stars phase array radar antenna," *IEEE Aerosp. Electron. Syst. Mag.*, pp. 34–41, Oct. 1994.

[17] J. Wood and D. Barry, "Linear signal synthesis using the Radon–Wigner transform," *IEEE Trans. Signal Processing*, vol. 42, pp. 2105–2111, Aug. 1994.

[18] L. Cohen, *Time-Frequency Analysis*. Upper Saddle River, NJ: Prentice-Hall, 1995.

[19] S. Qian and D. Chen, *Joint Time-Frequency Analysis: Methods and Applications*. Englewood Cliffs, NJ: Prentice-Hall, 1996.

[20] X.-G. Xia, "On estimation of multiple frequencies in undersampled complex valued waveforms," *IEEE Trans. Signal Processing*, vol. 47, pp. 3417–3419, Dec. 1999.

[21] G. C. Zhou and X.-G. Xia, "Multiple frequency detection in undersampled complex-valued waveforms with close multiple frequencies," *Electron. Lett.*, vol. 33, no. 15, pp. 1294–1295, July 1997.

[22] X.-G. Xia, "An efficient frequency-determination algorithm from multiple undersampled waveforms," *IEEE Signal Processing Lett.*, pp. 34–37, Feb. 2000.

[23] J. H. McClellan and C. M. Rader, *Number Theory in Digital Signal Processing*. Upper Saddle River, NJ: Prentice-Hall, 1979.

[24] D. C. Munson, Jr., J. D. O'Brien, and W. K. Jenkins, "A tomographic formulation of spotlight-mode synthetic aperture radar," *Proc. IEEE*, vol. 71, pp. 917–925, 1983.

[25] R. Fiedler and R. Jansen, "Adventures in SAR processing," in *Proc. SPIE*, Apr. 2000.

[26] R. Bamler, "A comparison of range-Doppler and wave number domain SAR focusing algorithms," *IEEE Trans. Geosci. Remote Sensing*, vol. 30, pp. 706–713, July 1992.

[27] W. M. Brown and R. J. Fredricks, "Range-Doppler imaging with motion through resolution cells," *IEEE Trans. Aerosp. Electron. Syst.*, vol. AES-5, pp. 98–102, 1969.

[28] S. R. Cloude and K. P. Papathanassiou, "Polarimetric SAR interferometry," *IEEE Trans. Geosci. Remote Sensing*, vol. 36, pp. 1551–1565, Sept. 1998.

[29] M. Soumekh, "Moving target detection in foliage using along track monopulse synthetic aperture radar imaging," *IEEE Trans. Image Processing*, vol. 6, pp. 1148–1161, Aug. 1997.

[30] G. Wang, X.-G. Xia, V. C. Chen, and R. L. Fiedler, "Detection, location and imaging of fast moving targets using multi-frequency antenna array SAR(MF-SAR)," in *Proc. EUSAR'2000*, May 2000, pp. 557–560.

[31] H. A. Zebker and J. Villasenor, "Decorrelation in interferometric radar echoes," *IEEE Trans. Geosci. Remote Sensing*, vol. 30, pp. 950–959, Sept. 1992.

[32] J. G. Fleischman, S. Ayasli, E. M. Adams, and D. R. Gosselin, "Foliage penetration experiment, Part I: Foliage attenuation and backscatter analysis of SAR imagery," *IEEE Trans. Aerosp. Electron. Syst.*, vol. 32, pp. 135–144, Jan. 1996.

[33] M. F. Toups, S. Ayasli, and J. G. Fleischman, "Foliage penetration experiment, Part II: Analysis of foliage-induced systhetic pattern distortions," *IEEE Trans. Aerosp. Electron. Syst.*, vol. 32, pp. 145–155, Jan. 1996.

[34] J. G. Fleischman, M. A. Worris, S. Ayasli, E. M. Adams, and D. R. Gosselin, "Foliage penetration experiment, Part III: Multichannel whitening of SAR imagery," *IEEE Trans. Aerosp. Electron. Syst.*, vol. 32, pp. 156–166, Jan. 1996.

[35] J. S. Lee, K. W. Hoppel, S. A. Mango, and A. R. Miller, "Intensity and phase statistics of multilook polarimetric and interferometric SAR imagery," *IEEE Trans. Geosci. Remote Sensing*, vol. 32, pp. 1017–1028, Sept. 1994.

Genyuan Wang received the B.S. and M.S. degrees from Shaanxi Normal Univerity, Xi'an, China, in 1985 and 1988, respectively, and the Ph.D. degree from Xidian University, Xian, China.

From 1993 to 1998, he was an Associate Professor of Shaanxi Normal University. Since June 1998, he has been with the Department of Electrical and Computer Engineering, University of Delaware, Newark, as a Postdoctoral Research Fellow. His research interests are communication systems including equalization and coding, signal processing, and its applications in SAR and ISAR imaging.

Xiang-Gen Xia (M'97–SM'00) received the B.S. degree in mathematics from Nanjing Normal University, Nanjing, China, the M.S. degree in mathematics from Nankai University, Tianjin, China, and the Ph.D. degree in electrical engineering from the University of Southern California, Los Angeles, in 1983, 1986, and 1992, respectively.

He was a Senior/Research Staff Member at Hughes Research Laboratories, Malibu, California, from 1995 to 1996. In September 1996, he joined the Department of Electrical and Computer Engineering, University of Delaware, Newark, where he is a Professor. He is currently also a Visiting Professor at the Chinese University of Hong Kong. Before 1995, he held visiting positions in a few institutions. His current research interests include digital communication systems and signal and image processing. He has over 90 refereed journal articles published, as well as five U.S. patents awarded. He is the author of the book *Modulated Coding for Intersymbol Interference Channels* (New York: Marcel Dekker, 2000). He is an Associate Editor of the *EURASIP Journal of Applied Signal Processing*, and he was a Guest Editor of "Space-Time Coding and Its Applications" in the *EURASIP Journal of Applied Signal Processing* in 2002.

Dr. Xia received the National Science Foundation (NSF) Faculty Early Career Development (CAREER) Program Award in 1997, the Office of Naval Research (ONR) Young Investigator Award in 1998, and the Outstanding Overseas Young Investigator Award from the National Nature Science Foundation of China in 2001. He also received the Outstanding Junior Faculty Award of the Engineering School of the University of Delaware in 2001. He is an Associate Editor of the IEEE TRANSACTIONS ON MOBILE COMPUTING, the IEEE SIGNAL PROCESSING LETTERS, the IEEE TRANSACTIONS ON SIGNAL PROCESSING. He is also a Member of the Signal Processing for Communications Technical Committee of the IEEE Signal Processing Society.

Victor C. Chen received the Ph.D. degree in electrical engineering from Case Western Reserve University, Cleveland, OH.

Since 1990, he has been with Radar Division, U.S. Naval Research Laboratory, Washington DC. His research interests include radar imaging, moving target detection, and time-frequency applications to radar. He has more than 90 publications in books, journals, and proceedings, including a recent book *Time-Frequency Transforms for Radar Imaging and Signal Analysis* (Boston, MA: Artech House, 2002).